

Article

Sulfate-Dependent Shear Behavior of Cementing Fiber-Reinforced Tailings and Rock

Xiangqian Xu ^{1,2} , Weilv Wu ¹ and Wenbin Xu ^{1,*}

¹ School of Energy and Mining Engineering, China University of Mining and Technology (Beijing), Beijing 100083, China; xiangqian20062006@126.com (X.X.); Weilv_Wu@163.com (W.W.)

² Department of Civil Engineering, University of Ottawa, 161 Colonel By, Ottawa, ON K1N 6N5, Canada

* Correspondence: xuwenbin@cumt.edu.cn

Received: 9 October 2020; Accepted: 16 November 2020; Published: 19 November 2020



Abstract: A better understanding of the shear behavior of the interface between cemented paste backfill (CPB) and the surrounding rock is critical for constructing cost-effective, durable, and reliable CPB structures. In practice, CPBs suffer sulfate attack during their service life, and as a typical cementitious material, the CPB itself has disadvantages, such as high brittleness, easy cracking, and insufficient durability, which restrict the further popularization and application of CPB technology. Thus, in this study, direct shear tests, electrical conductivity (EC) and thermal gravity/differential thermal gravimetric (TG/DTG) analyses were conducted to research the effects of different amounts of monofilament polypropylene fibers (0%, 0.1%, 0.3%, and 0.5%; by mass of the sum of the dry tailings and cement) and initial sulfate concentrations (0 mg/L, 5000 mg/L and 25,000 mg/L) on the shear behavior of the fiber-reinforced CPBs and rock (FR-CPB/rock) interface, and the Mohr–Coulomb shear envelop was used to fit the shear strength of specimens with various periods (1 day, 3 days, 7 days, and 28 days) under various stresses (50 kPa, 100 kPa, 150 kPa). The experimental testing results indicated that the fibers generally enhance the performance of the shear behavior of the FR-CPB/rock interface and the optimal fiber content correlates to the initial sulfate concentration. For the same treatment time (7 days), a fiber content of 0.1% contributes to the best shear performance for the FR-CPB/rock interface with a sulfate concentration of 5000 mg/L. For the sulfate-free and 25,000 mg/L concentration specimens, 0.3% is the optimal fiber content. Furthermore, for the studied interface specimens, sulfate content can play a positive (the refinement of the pore structure) or negative (the sulfate retardation effect) role in the interface shear behavior between the FR-CPB and rock, depending on the treatment time, the initial sulfate concentration, and the fiber content. For the specimens treated for 7 days and 28 days, the specimens with initial sulfate concentrations of 5000 mg/L and 25,000 mg/L achieved the highest peak shear strengths, respectively. The outcomes of this paper present a substantial reference for the design and optimization of underground FR-CPB structures under sulfate attack.

Keywords: shear behavior; sulfate concentration; geotextiles; geomembranes and geogrids; rock; interface

1. Introduction

Mineral resources provide a substantial material guarantee for human survival and social development. However, they also inevitably produce a series of problems such as environmental pollution and ecological damage during exploitation and utilization processes. Solid waste and goafs are considered major sources of disasters (mainly non-coal mines) [1]. For instance, in Sweden, approximately 20 million tons of tailings and 25 million tons of waste rock generated each year [2]. By comparison, China, the tailings produced by key industrial enterprises amounted to about

880 million tons in 2018, of which only 27.1% was reused [3]. These solid wastes not only add extra management cost to mining enterprises but also can easily induce a variety of geological ramifications (landslides, debris flows, surface collapse, and destruction of aquifers), thus leading to broader environmental and social problems. Cemented paste backfill (CPB) technology can reclaim the recovered mining solid waste into the goaf exploited previously to provide secondary support for the underground stope. Furthermore, it can also improve the recovery rate of mineral resources and reduce surface subsidence. Therefore, CPB has received widespread attention. With the government agencies' increasing environmental protection requirements for mining companies and increasing public awareness of environmental protection, CPB technology has become an important means to achieve safe, efficient, economic, and sustainable development of mineral resources [4–8]. (The main nomenclatures of the paper are summarized in Table 1.)

Table 1. Nomenclature table.

List of Symbols	Complete Terms
CPB	Cemented Paste Backfill
FR-CPB	Fiber-reinforced CPB
FR-CPB/rock interface	Interface between the FR-CPB and the rock.
UCS	Unconfined compressive strength
LVDT	Linear Variable Differential Transformer
ST	Silica tailings
TG	Thermal gravity
DTG	Differential thermal gravimetric
EC	Electrical conductivity
SEM	Scanning electron microscopy
C ₃ A	3CaO·Al ₂ O ₃
C-S-H	Calcium silicate hydrate

CPBs usually consist of dewatered or filtered tailings (78–85% of total mass), binder (generally 3–7% of total mass), mixed water (industrial or mine treated water), and additives (pumping agent, early strength agent, water reducing agent, and retarder). After being mixed on the ground to a design proportion, the CPB is transported to the working place through pumping or gravity [9,10]. The main function of the CPB is as a self-supporting artificial pillar and stope support structure. Therefore, its mechanical properties have always been a key issue during the CPB's service life. The traditional calculation of the target strength of the CPB was originally developed from soil mechanics, in which the shear strength behavior of the CPB is regarded as that of consolidated soil [11]. Subsequently, many researchers have focused on the mechanical strength evolution of CPBs under different conditions based on analytical calculations and numerical simulations [12–18]. However, a crucial aspect that has been ignored is the shear behavior of the interface between the CPB and the surrounding rock. When the CPB is filled into the goaf, it will yield downward under gravity. Because the stiffness of CPBs (0.1–1.2 GPa) differ greatly from those of rocks (20–100 GPa) [19], the shear force between the CPB and the surrounding rock will balance part of the self-weight stress, which will transform part of the self-weight stress into horizontal stress, resulting in the reduction of the vertical stress on the CPB. This phenomenon is known as the arching effect [20] (Figure 1). The arching effect was first proposed in the design of sand pile foundations, and then it was widely used in the design of retaining walls and trenches in the field of civil engineering [21–23]. In narrow backfill stopes (where the length to width ratio of the stope is greater than 5), the arching effect is more evident, and the conversion rate of the vertical stress and horizontal stress reaches up to 86.25% [24]. In other words, when the arching effect is taken into consideration, the target strength of the CPB can be achieved with less cement than usual. Cement is the commonly used binder agent, the cost of which can account for more than 75% of the CPB [25]. Therefore, a better understanding of this arching effect,

especially the shear behavior of the CPB–rock interface, allows for the design of a more economic and safer CPB structure.

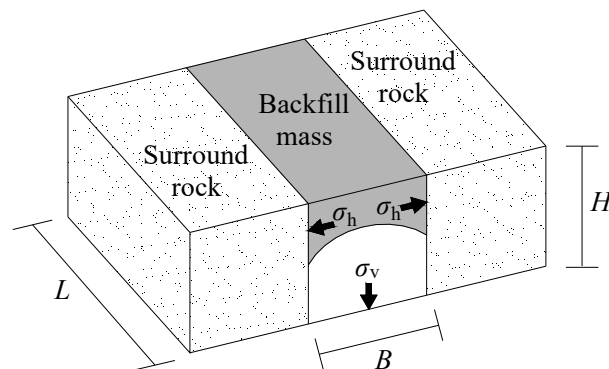


Figure 1. Schematic diagram of the arching effect (B: Stope width; L: Stope length; H: Layer height).

Few experimental studies have been performed to investigate the shear behavior of the CPB–rock interface [4,20,26–30]. These studies have mainly concentrated on the external conditions, such as the normal stress, curing time, curing temperature, and sulfate attack. None of these studies have focused on the mechanical properties of the CPB material itself. As with any typical cement-based material, CPB presents disadvantages with high brittleness, poor crack resistance, and poor durability [31,32]. These disadvantages can result in the instability or failure of a CPB structure, which could endanger the working environment and disturb the normal production sequence of mining enterprises [33]. Polypropylene fiber is a synthetic material, which is widely used because of its easy processing, and acid and alkali resistance [34]. Several studies have shown that adding polypropylene fibers to cement, concrete, and other materials can increase the strength, toughness, and ductility of the material and can improve the mechanical properties of the material. The main functions of polypropylene fiber in cement-based composite materials are improved crack resistance, reinforcement, and toughening. The reinforcement effect is related to the fiber’s orientation, length to diameter ratio, volume content, adhesion with the cement-based material matrix, and other factors [35–39]. The cemented filling material is significantly different from fiber-reinforced cement and fiber-reinforced concrete because of its tailings size, mineral composition, pore distribution, water to cement ratio, and other factors. Consequently, there is an urgent necessity to address the knowledge gap concerning the interface shear properties between fiber-reinforced CPB (FR-CPB) and rock in terms of the mechanical properties of the CPB material itself.

In addition, sulfate attack is inevitable during the service life of CPB structures due to numerous sources. The main sources of sulfate ions include the oxidation of sulfur-containing tailings (e.g., FeS_2 , CuFeS_2 , ZnS , and PbS), the use of mine processed tailwater as the mixing water, the oxidation of cyanide (particularly in some gold mines), and the insertion of some additives such as gypsum or anhydrite to decrease the setting time [7]. To the best of our knowledge, there are a lot studies on the effect of fiber [33–39] and the sulfate [7,9,10] content on the CPB, and the shear behavior of the CPB/rock interface [26–30] has been researched. Nevertheless, no investigations have been conducted on the shear behavior of FR-CPB and the rock interface considering the influence of sulfate attack. To overcome this knowledge gap, a series of direct shear tests were carried out to better understand the effects of the initial sulfate concentration on the shear property of the interface between the FR-CPB and the rock.

The main objectives of this paper are as follows:

- (1) To study the effect of the initial sulfate concentration on the behavior of a 1-day-old FR-CPB and rock interface;
- (2) To evaluate the effect of treatment time and the initial sulfate concentration on the behavior of the FR-CPB and rock interface (1-, 3-, 7-, and 28-day-old interface);

- (3) To compare the effect of the initial sulfate concentration on the interface behavior of FR-CPB material with various fiber contents (after 7 days of curing);
- (4) To develop a basic understanding of the shear behavior of the FR-CPB/rock interface under sulfate attack.

2. Experimental Program

2.1. Materials

The materials used in this study included tailings, binder, granite rock, monofilament polypropylene fibers (Adfil-Ignis), and water.

2.1.1. Tailings

The physical and chemical properties of the tailings mainly depend on the type of parent rock, the mineral composition, and the process used to extract the valuable components [15]. The tailings used in this experiment were ground artificial tailings produced by the U.S. Silica Co. (Figure 2a). The main components of the tailings were inert SiO_2 (99.8%) and other small amounts of compound, including aluminum oxide ($\text{Al}_2\text{O}_3 = 0.05\%$) and iron III oxide ($\text{Fe}_2\text{O}_3 = 0.035\%$). The use of these tailings eliminates the influence of the uncontrollable factors in natural tailings, to allow for a controlled case of evaluation [40]. The physical properties of the silica tailings (ST) material are measured by a Microtra S3500 Laser Particle Size Analyzer, shown in Table 2 in comparison with properties averaged from nine metal tailings in eastern Canada. The gradation properties of the ST material are similar to the properties of the metal tailings from eastern Canada, and they are referred to as medium-sized tailings.

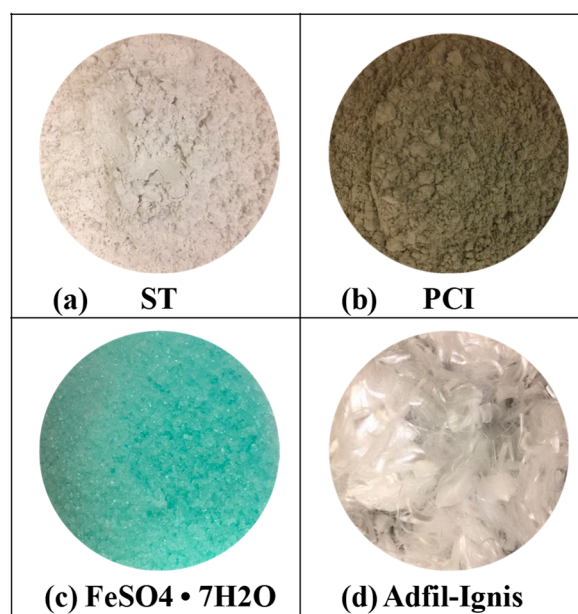


Figure 2. Test materials: (a) silica tailings (ST), (b) Ordinary Portland Cement Type I (PCI), (c) ferrous sulfate heptahydrate ($\text{FeSO}_4 \cdot 7\text{H}_2\text{O}$), (d) monofilament polypropylene fibers (Adfil-Ignis).

Table 2. Physical properties of the tailings.

Element	G_s	D_{10}	D_{30}	D_{50}	D_{60}	C_U	C_C	S_s
Unit	-	(μm)	(μm)	(μm)	(μm)	-	-	(cm^2/g)
ST	2.7	1.9	9.0	22.5	31.5	16.6	1.3	3600
Average properties of 9 types of tailings in eastern Canada	-	1.8	9.1	20.0	30.8	17.1	1.7	-

ST: silica tailings; G_s : specific gravity; C_U : coefficient of uniformity; C_C : coefficient of curvature; S_s : specific surface area.

2.1.2. Binder

Portland cement is the most used cementing material, and its physical and chemical properties and hydration reaction process have been well documented. Ordinary Portland Cement Type I (PCI) manufactured by Ciment Québec Inc. (Saint-Basile, QC, Canada) was used in this experiment (Figure 2b). The main physical and chemical properties of the PCI are presented in Table 3.

Table 3. Primary chemical and physical properties of the PCI used.

Binder	MgO (wt.%)	CaO (wt.%)	SiO ₂ (wt.%)	Al ₂ O ₃ (wt.%)	Fe ₂ O ₃ (wt.%)	SO ₃ (wt.%)	G _s	S _s (cm ² /g)
PCI	2.65	62.86	18.03	4.53	2.70	3.82	3.15	1300

G_s: Specific gravity; S_s: Specific surface area.

2.1.3. Rock Specimens

Granite samples cut using a special rock cutter to the required dimensions (60 mm × 60 mm × 10 mm) were used in this study. The average unconfined compressive strength (UCS) of the granite was 160 MPa. The rock surface in contact with the FR-CPB was flat and smooth according to the profile roughness parameter R_I [26]. In order to guarantee a good binding force between the FR-CPB and the granite interface, the rock samples were cleaned carefully before the sample preparation. Although roughness is a factor that can affect the interface behavior between dissimilar materials [28,41], it was not considered in the scope of this study.

2.1.4. Mixing Water

Distilled water mixed with a specific amount of ferrous sulfate heptahydrate (FeSO₄·7H₂O) was used in this study. The water-to-cement ratio (w/c) was 7.35, and the sulfate concentrations were 0 mg/L, 5000 mg/L, and 25,000 mg/L (Figure 2c).

2.1.5. Fibers

Monofilament polypropylene fibers (Adfil-Ignis) were used to reinforce the CPB (Figure 2d). The Adfil-Ignis fibers are composed of a milky white crystalline material with a neat structure. The fibers are 6 mm long and 18 μm in diameter, with a tensile strength of 600 MPa and a specific gravity of 0.91. Based on related studies performed on fiber reinforced cementitious materials [42–44], the fiber contents adopted in this study are 0%, 0.1%, 0.3%, and 0.5% by mass of the sum of the dry tailings and cement.

2.2. Sample Preparation

The preparation of specimens consisted of three steps: mortar mixing, molding, and specimen curing. First, the binders, tailings, fibers, and mixing water were weighed to target proportions, and then they were put into a mixing pot and were stirred for about 7 min to obtain a homogeneous mixture. Then, the mixture was poured directly on top of the rock samples, which had been previously placed in a 60 mm × 60 mm × 30 mm metal mold. To make sure the FR-CPB and the rock were fully in contact with each other, manual vibration was required for about 30 times to eliminate the bubbles generated at the interface. Immediately after the vibration, the mold was wrapped with plastic film to prevent moisture evaporation. Finally, it was labelled and cured in a temperature-controlled space for the designated curing time. The specimens before and after being put inside the shear box are shown in Figure 3.

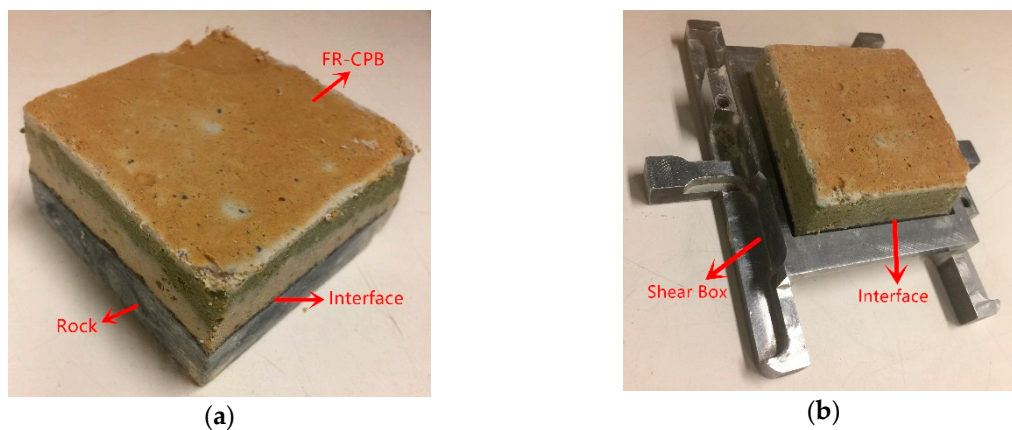


Figure 3. Specimen (a) before and (b) after being put inside the shear box.

2.3. Interface Shear Tests

The direct shear test was first used in slope stability studies by Alexandre Collin, and has since become widely used because of its simplicity and ease of operation [45]. The direct shear apparatus used in this experiment is a strain-controlled device. As shown in Figure 4, the linear variable differential transformers (LVDTs) were used to measure the vertical and horizontal displacements, and the load cell was used to measure the applied normal stress. The upper and lower parts of the shear box were loaded with the FR-CPB and rock, respectively. In addition, to ensure that the shear plane was present exactly at the interface, several steel beads were placed between the upper and lower parts of the shear box. During the test, a constant normal stress and shear rate were applied to the specimen. For each specimen, a shearing test was performed at three normal stresses (50 kPa, 100 kPa, and 150 kPa) to determine the Mohr–Coulomb shear parameters (interface friction angle and cohesion). In this experiment, the upper part of the shear box was fixed, and the lower part moved at a constant rate of 0.5 mm/min. In order to ensure the accuracy and repeatability of the experiment, each group of experiments was repeated at least three times. All the data from the test (shear force, shear and normal displacements) were collected using a computerized data logging system. The results were monitored and saved using LabView software (LabView2015). The details of the prepared mixes are summarized in Table 4.

Table 4. Recipes for the fiber-reinforced cemented paste backfill (FR-CPB)/rock interface specimens prepared in this study.

Specimen Type	Tailings	Binder Content (%)	W/C	Fiber Content (%)	Initial Sulfate Concentration (mg/L)	Treatment Time (Days)
FR-CPB/granite	ST	4.5	7.35	0	0, 5000, 25,000	1
FR-CPB/granite	ST	4.5	7.35	0.1	0, 5000, 25,000	7
FR-CPB/granite	ST	4.5	7.35	0.3	0, 5000, 25,000	1, 3, 7, 28
FR-CPB/granite	ST	4.5	7.35	0.5	0, 5000, 25,000	7

ST: silica tailings; W/C: mass of water divided by mass of binder; treated at room temperature (20 °C).

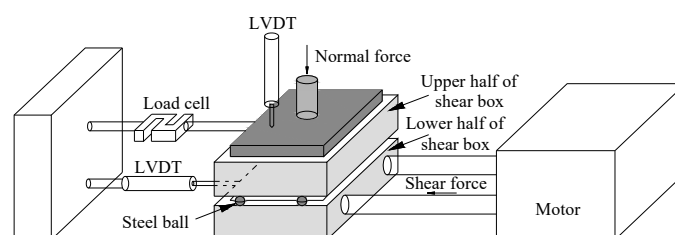


Figure 4. Schematic diagram of the direct shear device.

2.4. Microstructural Analyses

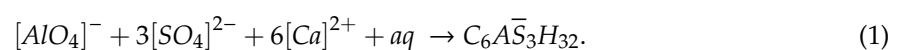
The mechanical properties of a CPB are, to some extent, the macroscopic response of its microstructure. To better understand the effect of the sulfate concentration on the shear characteristics of an FR-CPB and rock interface, thermal gravity (TG), differential thermal gravimetric (DTG), and electrical conductivity (EC) properties were used to analyze the microstructure of the specimens. The thermogravimetric analysis was used to study the weight loss and the thermal decomposition rate of the samples, while the electrical conductivity reflects the hydration of the cementitious materials and the corresponding microstructural evolution process by tracing the movement of ions.

Before the thermogravimetric analysis, the specimen was heated in an oven at 45–50 °C to remove any free moisture. After the weight of the specimen was stable for some time, the specimen was ground and screened. Then, it was packed in a sealed bag and put into a Q5000 V3.15 Build 263 thermogravimetric analyzer. The experimental gas used was nitrogen, and the reference material was alpha-Al₂O₃. The maximum heating range was 1000 °C. The electrical conductivity was measured using a 5TE sensor and an EM50 data logger system. The 5TE sensor measures the impedance between two electrodes using a dual probe array. The electrical conductivity measurement range is 0–7 ds/m with an accuracy of 0.01 ds/m.

3. Results and Discussion

3.1. Effects of Sulfate Concentration on the Shear Behavior of the Fiber-Reinforced Cemented Paste Backfill (FR-CPB)/Rock Interface

Figure 5 illustrates the evolution of the shear stress and shear displacement of the 1-day cured FR-CPB/rock interface specimens with various initial sulfate concentrations (0 mg/L, 5000 mg/L, and 25,000 mg/L) under a normal stress of 50 kPa, with 0% and 0.3% fiber contents. Results indicated that irrespective of the fiber content or the sulfate concentration, the shear stress increased with shear displacement up to a peak shear stress, after which the shear stress decreased until the residual shear strength was achieved. The FR-CPB/rock interface specimens without sulfate content exhibited strain softening characteristics (the shear stress increased to a distinct spike, and then sudden drop), while the specimens containing sulfate (5000 mg/L and 25,000 mg/L) exhibited strain hardening (the shear stress drop after peak is unobtrusive). Further, peak shear stress decreased and corresponding shear displacements increased with increasing sulfate content. These results are due to the retardation effect of sulfate on cementitious materials. It is well known that as an active ingredient in cement clinker, C₃A (3CaO·Al₂O₃) can react rapidly with sulfate ions to form ettringite (Equation (1)). This results in a protective film enveloping the surface of the unhydrated cement particles, which impedes the free flow and exchange of a portion of the active ions in the mixture slurry, thus inhibiting cement hydration [7,28,46–48]. This explanation can be verified experimentally using electrical conductivity measurements of the specimens, as shown in Figure 6. Results in Figure 6 demonstrate that the specimens which contain a higher amount of sulfate take longer to reach the maximum EC value, and this maximum EC value decreases as the sulfate concentration increases. For instance, the sulfate-free specimen reached a maximum EC value of 4.56 mS/cm within 0.13 d, while the specimens with 5000 mg/L and 25,000 mg/L of sulfate require 0.69 d and 1.37 d to reach their maximum EC values of 4.34 mS/cm and 3.42 mS/cm, respectively. These experimental results validate the inhibitory effect of sulfate on cement hydration. Furthermore, for specimens without sulfate content, the hydration products are mainly calcium silicate hydrate (C-S-H), which is the primary contributor to the strength of cementitious materials [49]. Thus, a stronger binding force will be achieved for the FR-CPB/rock interface specimens that does not contain sulfate. From the perspective of the hydration product, this is also another reason why the specimen without any sulfate can obtain a higher peak shear stress.



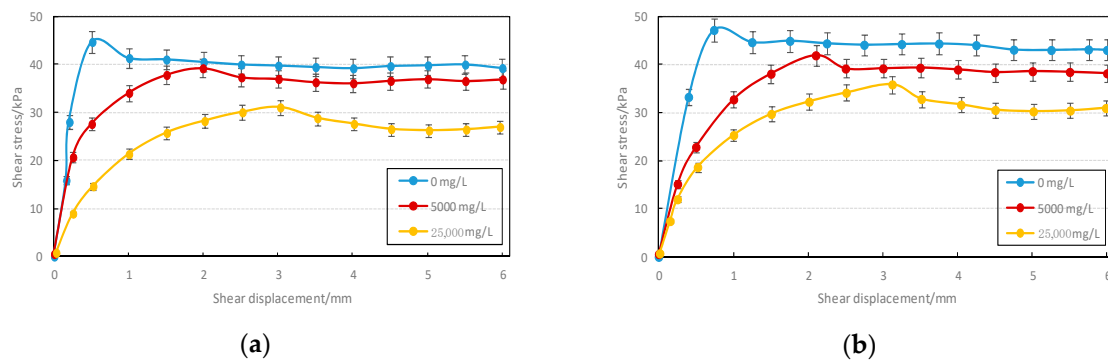


Figure 5. Shear stress vs. shear displacement curves of the FR-CPB/rock interface (treated for 1 day; normal stress of 50 kPa). (a) CPB made with 0% fibers; (b) CPB made with 0.3% fibers.

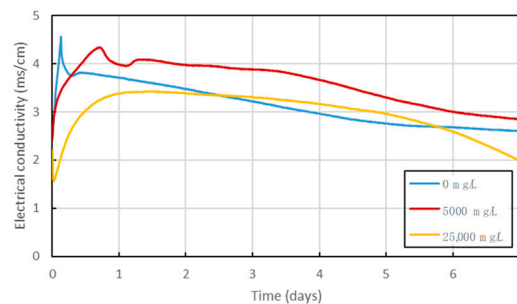


Figure 6. Variation in the electrical conductivity of the specimens with sulfate concentration (CPB made with 0.3% fibers).

Comparison of Figure 5a,b reveals that the specimens with 0.3% fibers have a higher peak shear stress and residual stress than the specimens without fibers, and the shear displacement corresponding to the peak shear strength of the former is larger than that of the latter. For instance, for the specimens with 0.3% fibers and sulfate concentrations of 0 mg/L, 5000 mg/L, and 25,000 mg/L, the peak shear stresses are 47.23 kPa, 41.93 kPa, and 35.87 kPa with corresponding shear displacements of 0.74 mm, 2.11 mm, and 3.13 mm, respectively. The peak shear stresses of the specimens with no fibers and sulfate concentrations of 0 mg/L, 5000 mg/L, and 25,000 mg/L are 44.75 kPa, 39.21 kPa, and 31.06 kPa with corresponding shear displacements of 0.51 mm, 1.99 mm, and 3.03 mm, respectively. These results are attributed to the reinforcing mechanism of the fibers in cementitious materials. It is well known that the fibers prevent the formation and propagation of microscopic and macroscopic cracks through bridging action [50–52]. The hydration process of cement-based materials leads to the evolution of the pore structure. Plastic settlement cracks and shrinkage cracks caused by self-desiccation are two main common microdefects in cementitious materials (the main source of internal stress), which are not conducive to the development of strength [27,53]. The dispersed fibers in the CPB matrix can bridge the CPB particles (tailings, cement hydration products). When subjected to an internal or external load, the inconsistency of the deformation due to the different elastic moduli leads to the tendency of mutual dislocation between the fibers and the CPB particles, thus forming an interfacial force between the fibers and the CPB particles. This interfacial force inevitably limits the relative slip of the fibers, allowing the fibers to bear a certain tensile stress and to share the load. Moreover, when the fibers are stressed, the CPB particles are restrained at the bending part of the fibers, which limits further deformation of the CPB particles. This interaction between the fibers and the CPB particles not only transfers and disperses the load but also increases the integrity and uniformity of the specimen [54,55]. Consequently, the reinforcing mechanism of the fibers ensures the enhancement of the overall peak shear stress and the corresponding shear displacement of specimens with 0.3% fibers.

Figure 7 is a plot of the vertical displacement versus the shear displacement of the 1-day FR-CPB/rock interface specimens with various initial sulfate concentrations (0 mg/L, 5000 mg/L,

and 25,000 mg/L) under a normal stress of 50 kPa. As shown in Figure 7, all of the curves exhibit substantial shear contracting at the beginning of the shearing (shear displacement ≤ 1.00 mm), which then decreases gradually with increasing shear displacement. This initially significant contraction occurs because for the specimens cured for only 1 day, the cement hydration is far from sufficient. Thus, fewer hydration products (e.g., C-S-H, CH, ettringite, gypsum) were produced, which led to infirm cementation between the tailing particles and the fibers themselves, as well as between the fibers and the CPB particles. The existence of C-S-H and expansive minerals, such as ettringite and gypsum (adequate but not excessive), determines the stability of the solid phase structure of cement-based materials [53]. This means that the specimens treated for 1 day exhibit a high compressibility. When the shear begins, more contact occurs between the FR-CPB matrix and the granite, and the large volumes of the local voids in the CPB matrix decrease [20]. Consequently, the specimens treated for 1 day exhibit compression in this stage. The relatively smaller amount of shear contraction in the subsequent stage can be interpreted as the gradual compaction of the voids mentioned above and the destruction of the asperities at the interface. These asperities are particularly weak when the specimens are subjected to a short curing time. Thus, these asperities can be easily destroyed during shearing [20,26]. The specimens containing sulfate also experience a higher degree of compression than the sulfate-free specimens, and a greater initial sulfate concentration leads to more compression. This is due to the sulfate retardation effect, which was previously discussed. The existence of sulfate retards the cement hydration reaction, resulting in fewer hydration products. Therefore, the specimens containing sulfate have a higher compressibility than those without sulfate. The retardation effect of sulfate can be intuitively observed during the experiment. Figure 8 shows the appearances of the specimens with a sulfate concentration of 25,000 mg/L after the direct shear experiment. There is a large amount of moisture that has not yet participated in the hydration reaction detained in the specimens. This phenomenon once again verifies the retardation effect of sulfate on cement hydration.

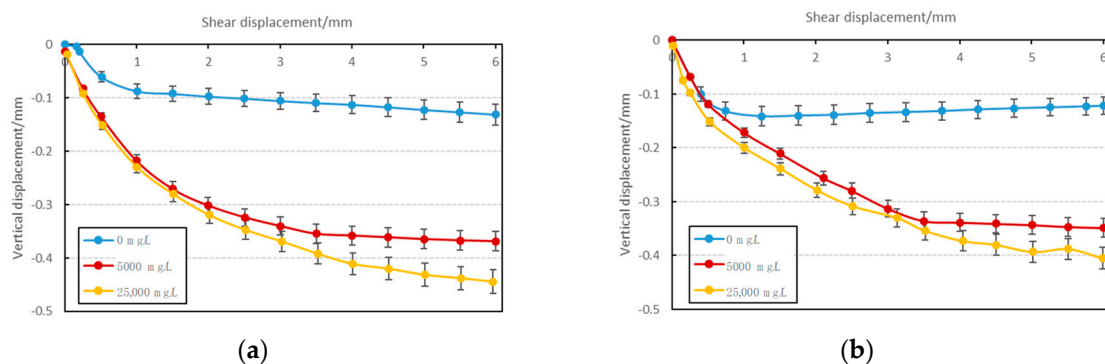


Figure 7. Vertical displacement vs. shear displacement curves of the FR-CPB/rock interface (treated for 1 day; normal stress of 50 kPa). (a) CPB made with 0% fibers; (b) CPB made with 0.3% fibers.



Figure 8. Specimens after the direct shear experiment (treated for 1 day; initial sulfate concentration of 25,000 mg/L; made with 0.3% fibers; normal stress of 50 kPa).

Comparison of Figure 7a,b reveals that the specimens with 0.3% fibers generally have less shear contraction than the specimens without fibers, and the sulfate-free specimens with 0.3% fibers exhibit some dilatation. This is because some of the voids or capillary pores in the CPB matrix are filled by the fibers, leading to an optimized pore structure. Therefore, the rearrangement of the fibers and the settlement of the CPB particles are restrained and, thus, less compressibility is observed on the macroscopic level [56]. The slight dilatancy mentioned above is caused by the relative movement of the asperities on the interface. Although only cured for 1 day, the specimens without sulfate still have a larger amount of hydration products than the sulfate containing specimens [28].

Figure 9 shows the evolution of the shear stress and shear displacement and the vertical displacement and shear displacement of the FR-CPB/rock interface specimens with various sulfate concentrations (cured for 1 day; CPB made with 0.3% fibers) under a normal stress of 150 kPa. Comparison of the results shown in Figures 5b and 7b, and Figure 9 reveals that irrespective of the initial sulfate concentration, the specimens subjected to a higher normal stress (150 kPa) have higher shear stresses and larger shear contraction than those subjected to a low normal stress (50 kPa), and no evidence of shear dilatancy was observed. This is because a higher normal stress will enlarge the contact area between the CPB particles and the granite and between the fibers and the granite. Accordingly, more friction is generated between the FR-CPB matrix and the rock, and thus, the shear stress is increased [26]. The larger shear contraction can be explained by the significantly reduced porosity and the greater compressibility of the specimens treated for a short time (1 day) when subjected to a higher normal stress. Moreover, the asperities and the larger CPB particles on the shear plane, which are still very weak due to the short curing time, can be easily destroyed or crushed under a higher normal stress, and thus the shear dilatancy is contained [20].

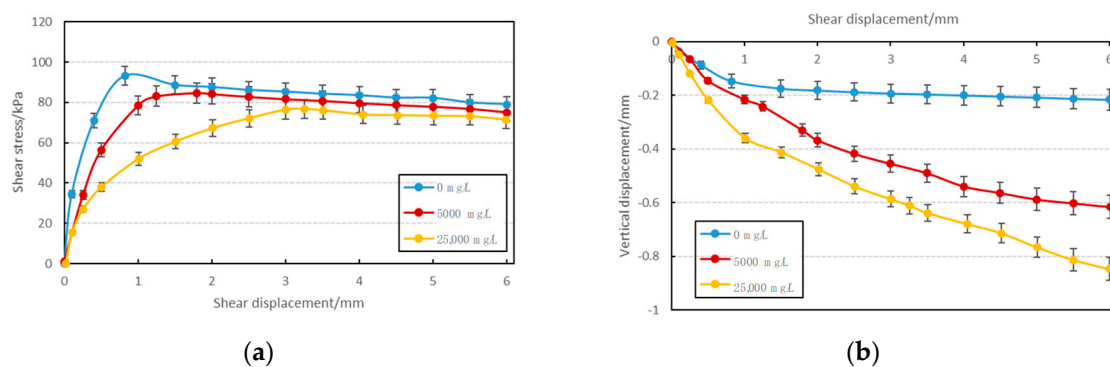


Figure 9. Shear properties of the specimens with various initial sulfate concentrations under a normal stress of 150 kPa (treated for 1 day; CPB made with 0.3% fibers). (a) shear stress vs. shear displacement. (b) vertical displacement vs. shear displacement.

Figure 10 shows the typical correlation between the peak shear stress and the normal stress of the 1-day old FR-CPB/rock interface specimens with various initial sulfate concentrations, which was acquired by fitting the peak shear stress and the corresponding normal stress of each group of specimens. As shown in the figure, all of the correlation coefficients R^2 of the envelope curves are greater than 0.97, and there is a good linear relationship between the shear strength and the normal stress irrespective of the sulfate content and the fiber content. This shear failure envelope can be well described by the Mohr–Coulomb criterion, where c and φ are the cohesion and internal frictional angle of the interface, respectively. The Mohr–Coulomb shear strength parameters (c and φ) are summarized in Table 5. This table once again verifies the sulfate inhibition and the fiber-reinforcing effect mentioned before.

$$\tau = \sigma_n \tan \varphi + c. \tag{2}$$

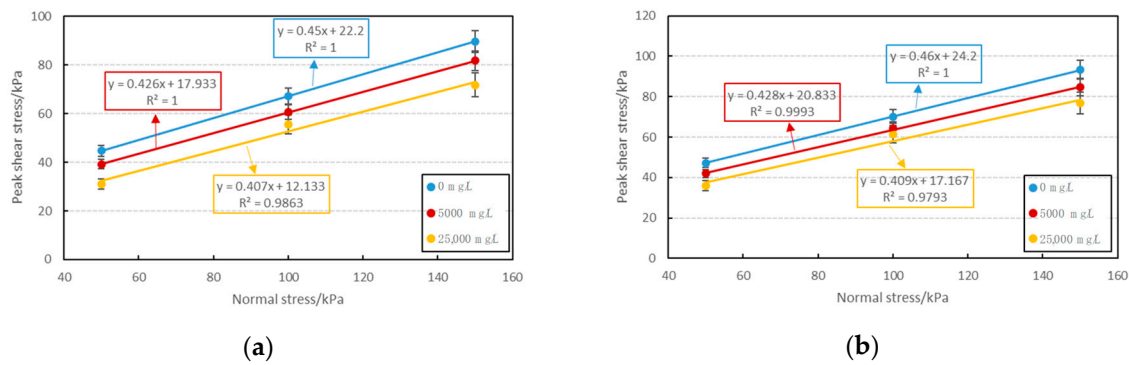


Figure 10. Plots of peak shear stress vs. normal stress for the 1-day old FR-CPB/rock interface specimens with various sulfate concentrations. (a) CPB made with 0% fibers; (b) CPB made with 0.3% fibers.

Table 5. Shear strength parameters of 1-day old interface specimens.

Sample Number	Interface Type	Fiber Content (%)	Sulfate Concentration (mg/L)	Interface Shear Strength Parameters	
				Cohesion, c (kPa)	Internal Friction Angle, φ (°)
1	FR-CPB/rock	0.0	0	22.2	24.2
2	FR-CPB/rock	0.0	5000	17.9	23.1
3	FR-CPB/rock	0.0	25,000	12.1	22.1
4	FR-CPB/rock	0.3	0	24.2	24.7
5	FR-CPB/rock	0.3	5000	20.8	23.2
6	FR-CPB/rock	0.3	25,000	17.2	22.2

3.2. Combined Effects of the Curing Time and the Initial Sulfate Concentration on the Shear Behavior of the FR-CPB/Rock Interface

Figure 11 illustrates the effect of the curing time on the shear stress versus shear displacement and the vertical displacement versus shear displacement of the FR-CPB/rock interface specimens with a sulfate concentration of 5000 mg/L (0.3% fiber content; normal stress of 100 kPa). As shown in Figure 11, a more extended curing time leads to a higher peak shear stress and corresponding higher shear deformation modulus. The shear contraction decreases with increasing curing time. This is because increasing curing time allows a more thorough cement hydration reaction, so more hydration products such as C-S-H and CH are generated [20,57]. Specimens cured for 28 days experienced a sudden bond failure at the interface (at a shear displacement of about 0.4 mm), then the shear stress decreased sharply, after which the shear stress increases once again until the residual shear stress is achieved. This sudden bond failure can be explained by the abrupt bond destruction of the entire cohesive interface when the peak shear stress is reached, which has also been reported in many previous studies [58,59]. During shearing, this phenomenon is accompanied by a clear audible sound.

Figure 12 depicts the coupled effects of the curing time and the initial sulfate concentration on the peak shear stress of the FR-CPB/rock interface. Results indicated that the peak shear stresses increases with increasing curing time, irrespective of the initial sulfate concentration. The reason for this is as discussed above; more hydration products are generated with increasing treatment time, which leads a stronger binding force between the FR-CPB matrix and the granite [20,26]. The main hydration product, C-S-H, also forms a more compact, harder structure. This leads to the formation of stronger asperities on the surface of the FR-CPB and, thus, a higher critical stress is needed to break these asperities [20,28]. Figure 12 also shows that the initial sulfate concentration has a non-negligible influence on the peak shear stress values and the rate of shear stress growth, as discussed below.

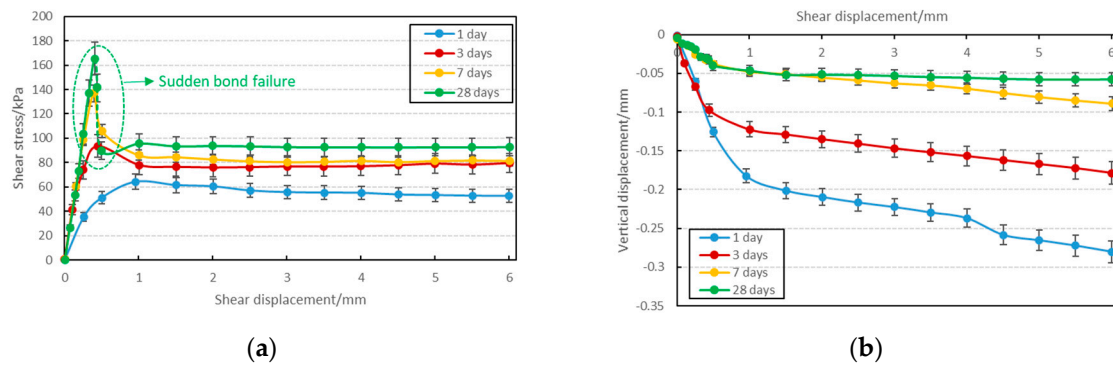


Figure 11. Plots of shear stress vs. shear displacement and vertical displacement vs. shear displacement of the FR-CPB/rock interface specimens treated for various periods (CPB made with 0.3% fibers; sulfate concentration of 5000 mg/L; normal stress of 100 kPa). (a) shear stress vs. shear displacement; (b) plots of vertical displacement vs. shear displacement.

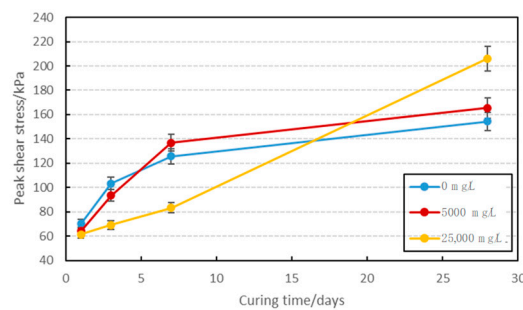


Figure 12. Coupled effects of treatment time and initial sulfate concentration on the evolution of the peak shear stress of the interface (CPB made with 0.3% fibers; normal stress of 100 kPa).

During the initial 3 days of curing, the sulfate-free specimens exhibited the highest peak shear stresses and shear stress growth rates. This is due to the sulfate retardation effect, as demonstrated through the TG/DTG analysis results shown in Figure 13 on specimens with sulfate concentrations of 0 mg/L and 25,000 mg/L, and cured for 3 days. As previously documented, the first peak weight loss that occurred between 30–105 °C is caused by the evaporation of the free moisture, while the second peak weight loss at 110–200 °C is due to the dewatering of the hydration products (e.g., C-S-H, ettringite, and gypsum), and the third peak weight loss at 400–450 °C and 600–750 °C is due to the disintegration of CH and calcite, respectively [28,60]. The TG/DTG analysis results indicated that the amount weight loss of the sulfate-free specimens at the first peak is less than that of the specimens with a sulfate concentration of 25,000 mg/L, which implies that there is more free moisture residue not involved in the cement hydration in the specimens containing 25,000 mg/L of sulfate. At the second peak, the weight loss is lower for the sulfate-free specimens, which implies that there are less hydration products (CH and calcite) in the sulfate containing specimen. In other words, the process of the cement hydration reaction has been retarded in the sulfate-containing specimen. These findings from the TG/DTG analysis again verifies the sulfate retardation effect on cement hydration, especially when the FR-CPB/rock interface specimen is subjected to a short curing time.

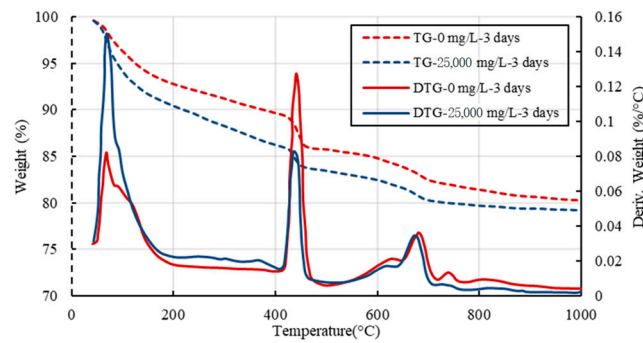


Figure 13. Thermal gravity/differential thermal gravimetric (TG/DTG) charts for specimens treated for 3 days with initial sulfate concentrations of 0 mg/L and 25,000 mg/L.

After one week of curing, the specimen with a sulfate concentration of 5000 mg/L exhibited the highest peak shear stress, followed by the specimens with sulfate concentrations of 0 mg/L and 25,000 mg/L (Figure 12). The higher peak shear stress of the 5000 mg/L sulfate containing specimen is attributed to the decrease in the porosity of the FR-CPB matrix. This is caused by the sedimentation of adequate, but not excessive, amounts of secondary expansive minerals (e.g., ettringite and gypsum), which are formed through the reaction between the sulfate ions and C_3A/CH , in the empty capillary pores of the FR-CPB matrix. This sedimentation helps optimize the pore structure of the FR-CPB matrix and makes the matrix more compact. Thus, the contact area between the FR-CPB matrix and the surface of the rock is increased, which results in a higher peak shear stress. This behavior has been well documented through scanning electron microscopy (SEM) imagery conducted on a sulfate containing CPB by several researchers [17,28,53,61,62]. These studies confirmed that moderate quantities of secondary expansive minerals precipitating in the empty capillary pores of the CPB are beneficial to the formation of a finer pore structure of the CPB, and it increases the strength of the CPB.

However, for 7-day cured specimens, the peak shear stress was the lowest for the 25,000 mg/L sulfate content specimens. It indicates that the positive effect of sedimentation caused by the secondary expansive minerals is also dependent on the initial sulfate concentration. The higher initial sulfate concentration induced more potent inhibitory effect, which even exceeds the refinement effect on the pore structure of the FR-CPB matrix. In addition, another factor responsible for the lower peak shear strength after 7 days of curing in the 25,000 mg/L sulfate containing specimen is the absorption of sulfate ions by C-S-H. It is well known that the state of the C-S-H is closely related to the chemical constituents in the ambient solution, and the existence of sulfate ions affects the morphological structure and mechanical response of the C-S-H. Specifically, the sulfate ions can be adsorbed by the C-S-H, and a higher sulfate concentration means a stronger absorbability [28,46]. This absorption can not only lead to the production of a lower quality or weaker C-S-H gel but to the promotion of a discrete acicular structure [63]. Thus, this absorption is not conducive to the strength progression of CPB or other cementitious materials in view of the fact that the strength of cementitious materials is chiefly dominated by C-S-H. In particular, the C-S-H provides the binding force to cohere with other hydration products [46,49]. In addition, several studies have focused on the interaction between sulfate ions and C-S-H from the microscopic perspective. For example, it has been reported that sulfate ion adsorption can significantly alter the CaO/SiO₂ ratio in C-S-H gel, thus further affecting the mechanical properties of C-S-H [64–66]. Other studies have pointed out that there is a linear correlation between the inherent strength of the C-S-H and its Ca/Si ratio, and the inherent strength increases with increasing Ca/Si ratio [67,68]. Still other studies report that the nucleation growth procedure of C-S-H can be influenced by sulfate ion absorption, which leads to a reduction in the interparticle forces between the C-S-H particles and thus the lower strength of sulfate containing cemented pastes [69]. It should be noted that considering the complexity of the C-S-H structure and its state, further research at the micro- or nano-scale is highly recommended to obtain a better knowledge of the sulfate ion absorption mechanism.

In contrast to the results on 7-day cured specimens, the 28-day cured specimens with 25,000 mg/L sulfate content exhibited peak shear strengths about 25% and 34% higher than that of 5000 mg/L and 0 mg/L sulfate content specimens, respectively. This finding seems to be contradictory to the explanation for the 25,000 mg/L sulfate containing specimen treated for 7 days, i.e., that the retardation effect on the cement hydration and the sulfate ion absorption by the C-S-H can negatively affect the strength development. In fact, for the specimens treated for 7 days, it can be safely concluded that two diametrically opposed mechanisms responsible for the strength development under sulfate attack co-exist, namely, a positive effect which leads to a strength increase (refinement of the pore structure of the FR-CPB matrix, sedimentation of more hydration products), and a negative effect, which leads to strength reduction (retardation of cement hydration, sulfate ion absorption by C-S-H). This behavior difference between 7 days and 28 days was also reported in previous studies [46,48]. The lower peak shear strength of the 5000 mg/L sulfate-containing specimen can be interpreted as being due to excessive quantities of secondary expansive minerals (ettringite and gypsum, which are formed through the reaction of sulfate ions with C_3A and CH, respectively), which impose excessive pressure on the pores of the FR-CPB matrix. This can lead to the formation of micro-fissures in the FR-CPB matrix. This can have several negative ramifications on strength growth, such as the formation of asperities with lower strength on the surface of the FR-CPB matrix, a reduction in the contact area between the FR-CPB matrix and the granite, and a lower binding force between the FR-CPB matrix and the surface of the granite [28]. This was experimentally verified by the results of the TG/DTG thermogravimetric analysis, as presented in Figure 14. Results indicated that the weight loss of the 5000 mg/L sulfate containing specimens at 400 °C and 450 °C (caused by the disintegration of CH) is higher than that of the 25,000 mg/L sulfate-containing specimens. This higher amount of CH means a more thorough cement hydration reaction, thus leading to excessive amounts of secondary expansive minerals (e.g., gypsum formed by the reaction of CH and sulfate ions) in the 5000 mg/L sulfate containing specimen. This results in excessive pressure on the pore structure of the FR-CPB matrix and, therefore, strength reduction.

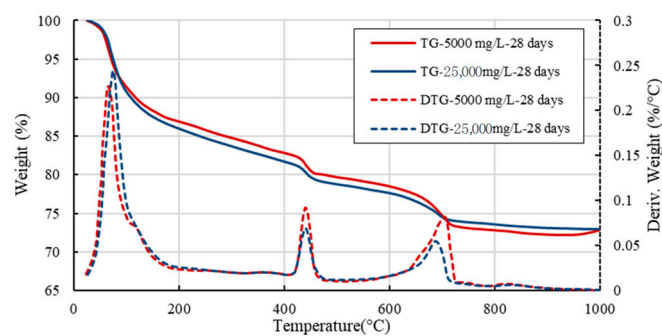


Figure 14. TG/DTG charts for specimens treated for 28 days with initial sulfate concentrations of 5000 mg/L and 25,000 mg/L.

Figure 15 presents the Mohr-Coulomb shear envelopes of the FR-CPB/rock interface specimens with a sulfate concentration of 5000 mg/L at four different curing times. Figure 16 shows the effect of curing time on shear strength parameters (c and f) of the FR-CPB/rock interface specimens at 0, 5000, and 25,000 mg/L initial sulfate concentrations. As shown in Figure 18, all of the curves agree well with the Mohr-Coulomb failure criterion, irrespective of the treatment time. Results indicated that the internal friction angle values and the cohesion increase with curing time, as expected. This increase is attributed to the more hydration products with increased treatment time [20,26,28,56]. Moreover, results indicated that the change in shear strength parameters with curing time depends on the initial sulfate concentration. For instance, the cohesion of the sulfate containing specimens decreases as the sulfate concentration increases for a 3-day treatment time, which is mainly due to the sulfate-induced retardation of the cement hydration process, as interpreted above. While for the 7-day

and 28-day treatments, the specimens containing 5000 mg/L and 25,000 mg/L of sulfate achieve the highest cohesion. This result reconfirm the inference above.

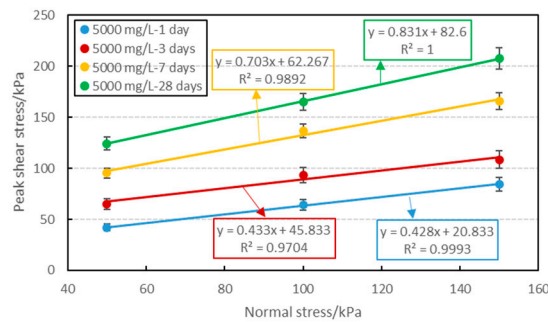


Figure 15. Shear envelopes of the FR-CPB/rock interface (CPB made with 0.3% fibers; sulfate concentration of 5000 mg/L).

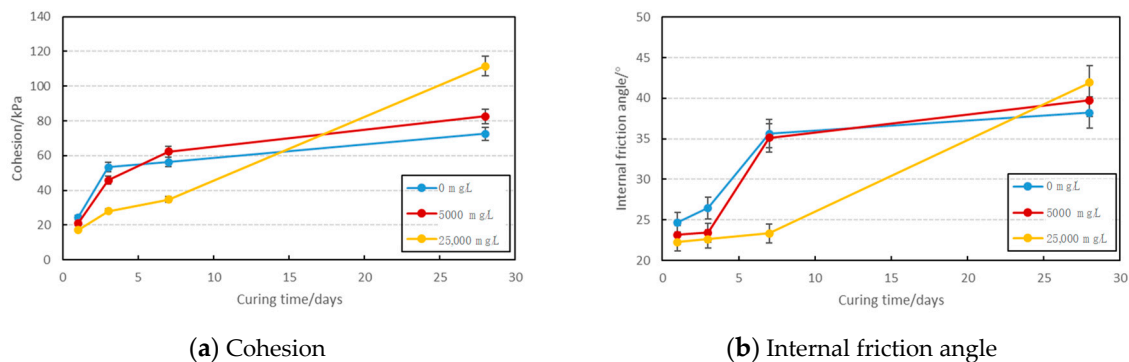


Figure 16. Evolution of the shear strength parameters of the FR-CPB/rock interface with sulfate concentration under the effect of treatment time (CPB made with 0.3% fibers).

The results described above once again verify the combined mechanisms of sulfate ions on the evolution of the shear properties of the studied interface as was explained previously, namely, the positive mechanism and the negative mechanism. Both of these mechanisms can positively or negatively affect the shear properties of the studied interface specimens; however, which one is dominant depends on the initial sulfate concentration and the treatment time. It should be noted that the evolution of the interface shear strength parameters significantly affects the arching effect, which was demonstrated by Fang and Fall [28]. Therefore, it is essential to obtain a better understanding of the combined mechanisms under sulfate attack in order to design economic and stable underground fiber-reinforced CPB structures.

3.3. Combined Effects of the Fiber Content and the Initial Sulfate Concentration on the Shear Behavior of the FR-CPB/Rock Interface

Figure 17 shows plots of the shear stress versus shear displacement and the vertical displacement versus shear displacement of FR-CPB/rock interface specimens cured for 7 days with different fiber contents and initial sulfate concentrations. Results indicated that the enhancement effect of the fibers on the FR-CPB/rock interface is dependent on the initial sulfate concentration. For the 5000 mg/L sulfate-containing specimen interface, the 0.1% fibers yielded the highest peak shear strengths and residual shear strengths, while for the 0 mg/L and 25,000 mg/L specimen interfaces, the 0.3% fibers yielded a better performance. In other words, there is an optimal fiber content that facilitates the shear properties of the FR-CPB/rock interface for a certain initial sulfate concentration. This result is consistent with those of previous studies performed on fiber-reinforced soils [43,55,70,71] and those conducted on fiber reinforced cementitious materials [42,56,72]. The optimal fiber content is largely dependent on its reinforcement efficiency. When a moderate amount of fibers is added to the CPB

matrix, the fibers can bridge the CPB particles (tailings, cement hydration products) and interweave with each other to form a three-dimensional stress transfer network. When one individual fiber is stressed, other fibers will inevitably be mobilized to share the load, and thus, the load can be distributed to a wider extent, and the reinforcing capability is further improved. However, if the fiber content is less than a certain threshold, the spacing between the fibers is too large to overlap with each other, and thus, an effective stress transfer network cannot be formed. If the fiber content is larger than this threshold, it will result in problems such as bundling, balling, and a decrease in workability. This results in a poor distribution of the fibers in the CPB matrix, which can lead to microdefects in the FR-CPB matrix and also a weaker bridging action between the fibers and the CPB particles, thus limiting the capability for the stress network to share the load [55,56,73]. We interpret the observed best performance to be for 0.3% fibers incorporated in a 0 mg/L and 25,000 mg/L sulfate-containing interface. The optimal fiber content of 0.1% for the 5000 mg/L sulfate containing interface is attributed to the combined mechanisms of (a) the sedimentation of adequate, but not excessive, amounts of secondary expansive minerals in the empty capillary pores of the FR-CPB matrix and on the surface of the FR-CPB/rock interface (already discussed above), and (b) the fiber-induced replacement of cement hydration products generated on the FR-CPB/rock interface. This replacement could lead to a decrease in the effective contact area between the FR-CPB matrix and the granite. Thus, the binding force and cohesion between the FR-CPB matrix and the granite decrease as well. A lower fiber content means a less severe replacement. Consequently, it is highly probable that aggregating large volumes of secondary expansive minerals and cement hydration products on the surface of the FR-CPB/rock interface for the 5000 mg/L specimen with 0.1% fibers is conducive to the binding force and cohesion of the interface and to the shear stress. This argument is verified by the results of the shear strength parameters presented in Figure 18 and by the SEM result presented by Xu et al., in which the replacement of the cement hydration products at the interface can be observed [56]. In addition, the lack of a dramatic distinction in the slope at the initial linear elasticity stage on all of the shear stress-shear displacement curves means that the fibers do not dramatically affect the initial stiffness of the specimens. This indicates that at this stage, the interface shear properties are chiefly determined by the binding force or the cementation between the FR-CPB matrix and the granite, and the fibers have not undertaken their role yet [56,70].

The vertical displacement versus shear displacement curves in Figure 17 reveal that the total amount of the shear deformation decreases with increasing fiber content. This is expected because the fibers restrain the rearrangement and settlement of the CPB particles, and thus they exert macroscopic constraints on the compressibility and further deformation of the FR-CPB matrix. Moreover, the lower volumes of fibers are not enough to fill the large voids and pores in the CPB material; while the larger amounts of fiber can be wrapped or interwoven into a network, which can fill the microcracks and capillary pores in the CPB matrix and limit the further deformation of the CPB material. This argument agrees well with the results of the study of fiber reinforced soft soil conducted by Starcher and Liu [74] and the study of fiber-reinforced CPB conducted by Xu et al. [56], in which they pointed out that the incorporation of fibers can reduce the compressibility.

Figure 18 depicts the effects of the fiber content and the initial sulfate concentration on the Mohr–Coulomb shear strength parameters of the FR-CPB/rock interface. The specimens with a sulfate concentration of 5000 mg/L yielded the highest cohesion, followed by the specimens with concentrations of 0 mg/L and 25,000 mg/L. The higher cohesion for the 5000 mg/L concentration specimen is due to the refinement of the FR-CPB pore structure caused by the sedimentation of adequate, but not excessive, amounts of secondary expansive hydration products, thus increasing the contact area between the FR-CPB and the granite, which in turn enhances the cohesion at the interface. While the lowest cohesion for the 25,000 mg/L concentration specimen is due to the strong retardation of effect of the sulfate ions on the cement hydration, resulting in fewer hydration products, thus decreasing the binding force at the interface. Figure 18b shows that the internal friction angle of the sulfate-free interface is generally higher than that of the sulfate containing specimens, and the internal friction angle decreases

as the sulfate concentration increases. This is because the aforementioned sulfate retardation results in the generation of weaker asperities on the surface of the FR-CPB, thus decreasing the friction at the interface [28].

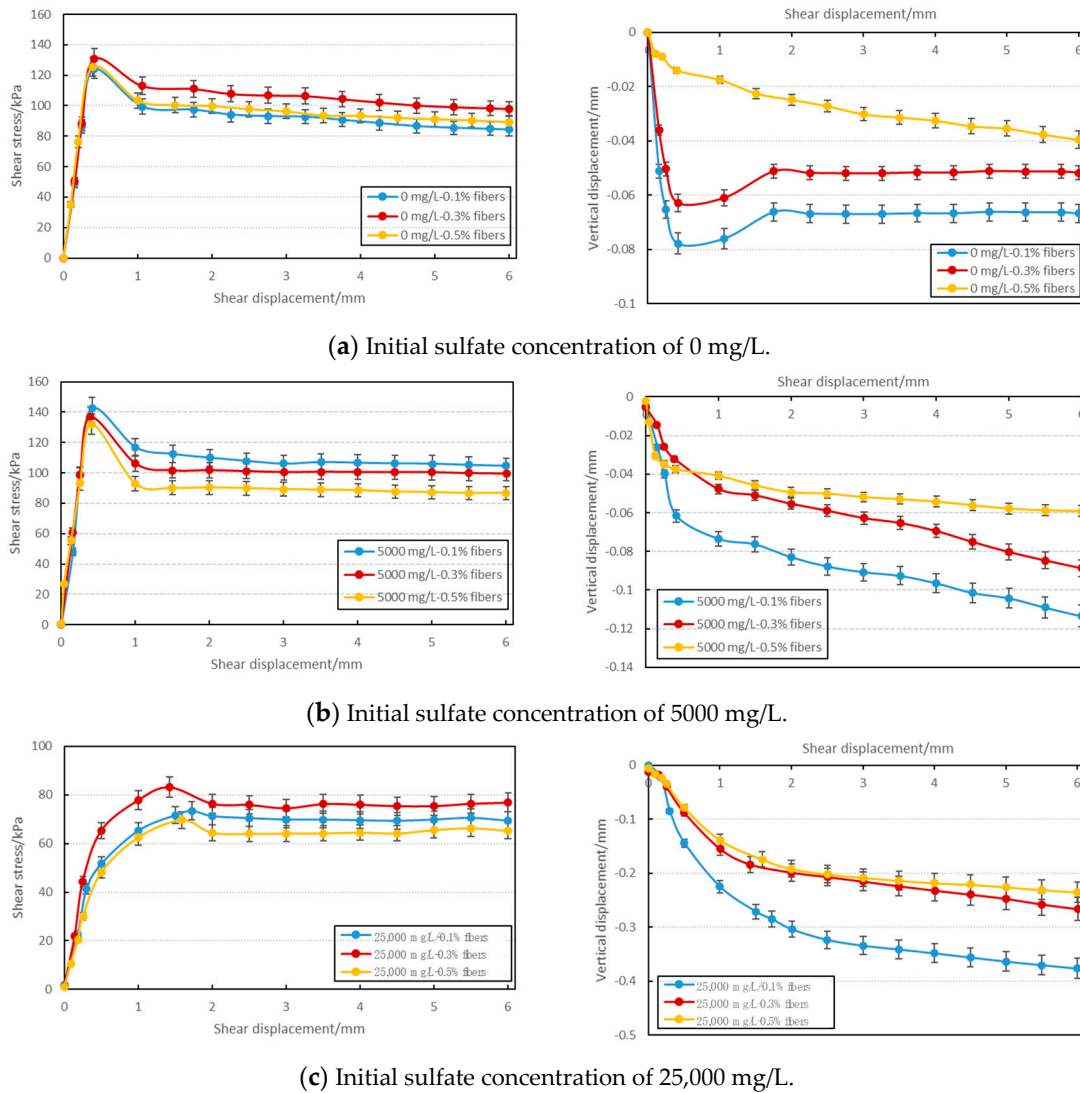


Figure 17. Plots of shear stress vs. shear displacement and vertical displacement vs. shear displacement of the FR-CPB/rock interface specimens with various fiber contents under the effect of the initial sulfate concentration (treatment time of 7 days; normal stress of 100 kPa).

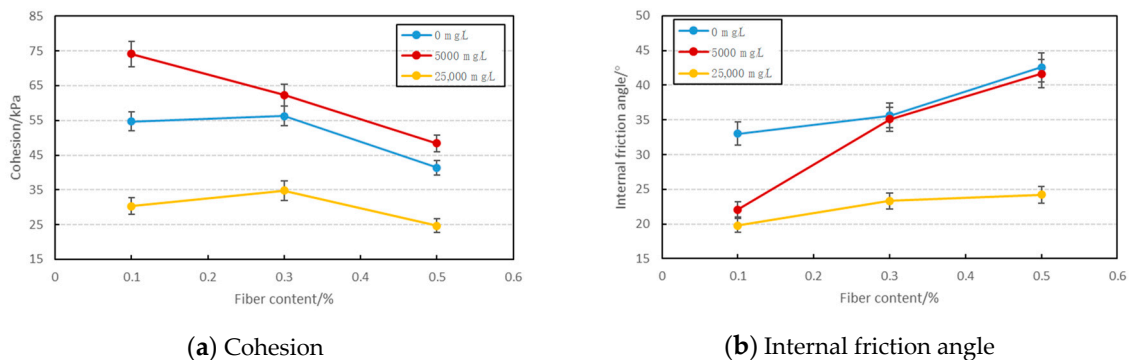


Figure 18. Effect of fiber content on the evolution of the shear strength parameters (cohesion and internal friction angle) of the FR-CPB/rock interface for various initial sulfate concentrations (treated for 7 days).

However, Figure 18 reveals that the sulfate-dependent evolution of the shear strength parameters of the FR-CPB/rock interface is also a function of the fiber content. Specifically, Figure 18a shows that for the 5000 mg/L concentration specimen, the 0.1% fiber content contributes to the acquisition of the highest cohesion, while for the sulfate-free and 25,000 mg/L concentration specimens, a 0.3% fiber content corresponds to the highest interface cohesion. Large volumes of fiber (0.5%) remarkably reduce the cohesion at the interface, regardless of the initial sulfate concentration. These findings again verify the aforementioned conclusions.

Figure 18b shows that the internal friction angle of the interface increases with increasing fiber content. This is because large quantities of fibers can interweave into a network and bridge the cracks formed in the asperities and postpone their development. Accordingly, an increase in the local shear stress is needed to completely damage these asperities, resulting in an increased interface frictional strength. In addition, it should be noted that the existence of fibers is an additional element responsible for the higher frictional strength as the fibers roughen the FR-CPB/rock interface, thus enhancing the frictional resistance at the interface [56].

4. Summary and Conclusions

In this study, experimental testing was performed on monofilament polypropylene fiber-reinforced CPB to evaluate the shear behavior and microstructural properties of the FR-CPB/rock interface, as a function of the initial sulfate concentration (0 mg/L, 5000 mg/L, and 25,000 mg/L), curing time (1 day, 3 days, 7 days, and 28 days), and the fiber content (0%, 0.1%, 0.3%, and 0.5%). Nearly 200 specimens were prepared and direct shear tests, thermogravimetric (TG/DTG) analysis, and electrical conductivity (EC) monitoring analysis were performed. Based on the performed tests, the following conclusions were drawn:

(1) Sulfate has two contradictory mechanisms that can significantly affect the shear properties of the interface between FR-CPB and granite. The positive function, which leads to an increase in the interface shear stress, is chiefly due to the refinement of the pore structure caused by the sedimentation of adequate, but not excessive, amounts of secondary expansive minerals within the empty pores of the FR-CPB matrix. The negative function, which results in a reduction in the interface shear stress, includes the sulfate-induced retardation of the cement hydration, the generation of weaker C-S-H caused by sulfate ion absorption, and the propagation of microcracks or the coarsening of the FR-CPB matrix induced by the sedimentation of excessive amounts of secondary expansive minerals. Which mechanism is dominant is largely dependent on the combined effects of the initial sulfate concentration, the treatment time, and the fiber content.

(2) A higher normal stress leads to a higher peak shear strength and a larger compressibility of the FR-CPB/rock interface. By fitting each set of normal stress and peak shear strength, it was determined that the shear failure envelope of the FR-CPB/rock interface agrees well with the Mohr–Coulomb failure criterion. The calculated shear strength parameters (cohesion and internal friction angle) are also dramatically influenced by the initial sulfate concentration, the treatment time, and the fiber content.

(3) An extended treatment time leads to a higher peak shear strength of the FR-CPB/rock interface. For the specimens treated for a short time (1 day and 3 days), the sulfate retards the cement hydration, thus resulting in a reduction in the peak shear strength. While for the specimens treated for 7 days and 28 days, the specimens with initial sulfate concentrations of 5000 mg/L and 25,000 mg/L achieved the highest peak shear strengths, respectively.

(4) The incorporation of fibers generally enhances the shear performance (peak shear strength and residual shear strength) of the FR-CPB/rock interface. However, the efficiency of this fiber enhancement is also a function of the initial sulfate concentration. For the same treatment time (7 days), a fiber content of 0.1% contributes to the best shear performance for the FR-CPB/rock interface with a sulfate concentration of 5000 mg/L. While for the sulfate-free and 25,000 mg/L concentration specimens, 0.3% is the optimal fiber content. Moreover, the existence of fibers limits the further deformation of

the FR-CPB/rock interface, and the magnitude of this vertical displacement decreases with increasing fiber content.

Author Contributions: Conceptualization, X.X.; methodology, X.X.; software, X.X.; validation, W.W.; formal analysis, W.W.; investigation, X.X.; resources, X.X.; data curation, X.X. and W.W.; writing—original draft preparation, X.X.; writing—review and editing, W.W.; visualization, W.W.; supervision, W.W.; project administration, W.X.; funding acquisition, W.X. All authors have read and agreed to the published version of the manuscript.

Funding: This research was funded by National Key Technologies Research & Development Program (2018YFE0123000), the Natural Sciences and Engineering Research Council of Canada, University of Ottawa and the China Scholarship Council, YueQi Young Scholar project, China (800015Z1185).

Conflicts of Interest: The authors declare no conflict of interest. The funders had no role in the design of the study.

References

1. Yilmaz, E. Advances in reducing large volumes of environmentally harmful mine waste rocks and tailings Introduction. *Gospod. Surowcami Miner. Miner. Resour. Manag.* **2011**, *27*, 89–112.
2. Swedish Waste Research Council. *Svensk Gruvavfallsforskning: Seminar 15 December 1998*; AFR Rapport 194, AFR-R-194-SE; AFN, Naturvårdsverket, Swedish Environmental Protection Agency: Stockholm, Sweden, 1998; ISSN 1102-6944. (In Swedish)
3. Current Situation of China's Large and Medium Municipal Solid Waste Pollution. Recycling of Bulk Industrial Solid Waste. 2020. Available online: <http://www.chyxx.com/industry/202007/882981.html> (accessed on 9 October 2020). (In Chinese).
4. Nabassé, J.F.; Koupouli, B.T.; Rivard, P.; Effenguet, H. Direct shear tests on cemented paste backfill–rock wall and cemented paste backfill–backfill interfaces. *J. Rock Mech. Geotech. Eng.* **2016**, *8*, 472–479.
5. Belem, T.; Benzaazoua, M. Design and application of underground mine paste backfill technology. *Geotech. Geol. Eng.* **2008**, *26*, 147–174. [[CrossRef](#)]
6. Orejarena, L.; Fall, M. Mechanical response of a mine composite material to extreme heat. *Bull. Eng. Geol. Environ.* **2008**, *67*, 387–396. [[CrossRef](#)]
7. Fall, M.; Benzaazoua, M. Modeling the effect of sulphate on strength development of paste backfill and binder mixture optimization. *Cem. Concr. Res.* **2005**, *35*, 301–314. [[CrossRef](#)]
8. Ghirian, A.; Fall, M. Coupled thermo-hydro-mechanical–chemical behaviour of cemented paste backfill in column experiments. Part I: Physical, hydraulic and thermal processes and characteristics. *Eng. Geol.* **2013**, *164*, 195–207. [[CrossRef](#)]
9. Benzaazoua, M.; Belem, T.; Bussière, B. Chemical factors that influence the performance of mine sulphidic paste backfill. *Cem. Concr. Res.* **2002**, *32*, 1133–1144. [[CrossRef](#)]
10. Benzaazoua, M.; Marion, P.; Picquet, I.; Bussière, B. The use of pastefill as a solidification and stabilization process for the control of acid mine drainage. *Miner. Eng.* **2004**, *17*, 233–243. [[CrossRef](#)]
11. Guo, G.L.; Zhu, X.J.; Zha, J.F.; Qiang, W. Subsidence prediction method based on equivalent mining height theory for solid backfilling mining. *Trans. Nonferr. Met. Soc. China* **2014**, *24*, 3302–3308. [[CrossRef](#)]
12. Mitchell, R.J.; Olsen, R.S.; Smith, J.D. Model studies on cemented tailings used in mine backfill. *Can. Geotech. J.* **1982**, *19*, 14–28. [[CrossRef](#)]
13. Cui, L.; Fall, M. Multiphysics modeling and simulation of strength development and distribution in cemented tailings backfill structures. *Int. J. Concr. Struct. Mater.* **2018**, *12*, 25. [[CrossRef](#)]
14. Lu, G.; Fall, M.; Yang, Z. An evolutive bounding surface plasticity model for early-age cemented tailings backfill under cyclic loading. *Soil Dyn. Earthq. Eng.* **2019**, *117*, 339–356. [[CrossRef](#)]
15. Wang, Y.; Fall, M.; Wu, A. Initial temperature-dependence of strength development and self-desiccation in cemented paste backfill that contains sodium silicate. *Cem. Concr. Compos.* **2016**, *67*, 101–110. [[CrossRef](#)]
16. Yilmaz, E.; Belem, T.; Benzaazoua, M. Effects of curing and stress conditions on hydromechanical, geotechnical and geochemical properties of cemented paste backfill. *Eng. Geol.* **2014**, *168*, 23–37. [[CrossRef](#)]
17. Pokharel, M.; Fall, M. Combined influence of sulphate and temperature on the saturated hydraulic conductivity of hardened cemented paste backfill. *Cem. Concr. Compos.* **2013**, *38*, 21–28. [[CrossRef](#)]
18. Cui, L.; Fall, M. Multiphysics modeling of arching effects in fill mass. *Comput. Geotech.* **2017**, *83*, 114–131. [[CrossRef](#)]
19. Shui, Z.H.; Zhang, R.; Chen, W.; Xuan, D.X. Effects of mineral admixtures on the thermal expansion properties of hardened cement paste. *Constr. Build. Mater.* **2010**, *24*, 1761–1767. [[CrossRef](#)]

20. Nasir, O.; Fall, M. Shear behaviour of cemented pastefill-rock interfaces. *Eng. Geol.* **2008**, *101*, 146–153. [[CrossRef](#)]
21. Tsai, J.S.; Chang, J.C. Three-dimensional stability analysis for slurry-filled trench wall in cohesionless soil. *Can. Geotech. J.* **1996**, *33*, 798–808. [[CrossRef](#)]
22. Take, W.A.; Valsangkar, A.J. Earth pressures on unyielding retaining walls of narrow backfill width. *Can. Geotech. J.* **2001**, *38*, 1220–1230. [[CrossRef](#)]
23. Pain, A.; Chen, Q.S.; Nimbalkar, S.; Zhou, Y. Evaluation of seismic passive earth pressure of inclined rigid retaining wall considering soil arching effect. *Soil Dyn. Earthq. Eng.* **2017**, *100*, 286–295. [[CrossRef](#)]
24. Wu, A.X.; Shen, H.; Jiang, L. Arching effect of long-narrow cemented paste backfill body and its effect on target strength. *Trans. Nonferr. Met. Soc. China* **2016**, *26*, 648–654.
25. Grice, T. Recent mine developments in Australia. In Proceedings of the 7th International Symposium on Mining with Backfill (MINEFILL), Seattle, WA, USA, 17–19 September 2001; pp. 351–357.
26. Fall, M.; Nasir, O. Mechanical behaviour of the interface between cemented tailings backfill and retaining structures under shear loads. *Geotech. Geol. Eng.* **2010**, *28*, 779–790. [[CrossRef](#)]
27. Fang, K.; Fall, M. Effects of curing temperature on shear behaviour of cemented paste backfill-rock interface. *Int. J. Rock Mech. Min. Sci.* **2018**, *112*, 184–192. [[CrossRef](#)]
28. Fang, K.; Fall, M. Chemically induced changes in the shear behaviour of the interface between rock and tailings backfill undergoing cementation. *Rock Mech. Rock Eng.* **2019**, *52*, 3047–3062. [[CrossRef](#)]
29. Fang, K.; Fall, M. Shear behavior of the interface between rock and cemented backfill: Effect of curing stress, drainage condition and backfilling rate. *Rock Mech. Rock Eng.* **2020**, *53*, 325–336. [[CrossRef](#)]
30. Hassani, F.P.; Mortazavi, A.; Shabani, M. An investigation of mechanisms involved in backfill-rock mass behaviour in narrow vein mining. *J. S. Afr. Inst. Min. Metall.* **2008**, *108*, 463–472.
31. Ling, T.C.; Kaliyavaradhan, S.K.; Poon, C.S. Global perspective on application of controlled low-strength material (CLSM) for trench backfilling—An overview. *Constr. Build. Mater.* **2018**, *158*, 535–548. [[CrossRef](#)]
32. Xu, W.; Li, Q.; Liu, B. Coupled effect of curing temperature and age on compressive behavior, microstructure and ultrasonic properties of cemented tailings backfill. *Constr. Build. Mater.* **2020**, *237*, 117738. [[CrossRef](#)]
33. Han, B.; Wu, A.X.; Deng, J.; Wang, X.L. Backfill technical analysis based on reliability theory in the underhand drift cut-and-filling stoping. *J. Cent. South Univ.* **2006**, *37*, 583–587.
34. Yu, C.; Zhu, M.; Shong, X.; Chen, Y. Study on dyeable polypropylene fiber and its properties. *J. Appl. Polym. Sci.* **2010**, *82*, 3172–3176. [[CrossRef](#)]
35. Song, P.; Hwang, S.; Sheu, B. Strength properties of nylon- and polypropylene-fiber-reinforced concretes. *Cem. Concr. Res.* **2005**, *35*, 1546–1550. [[CrossRef](#)]
36. Banthia, N.; Gupta, R. Influence of polypropylene fiber geometry on plastic shrinkage cracking in concrete. *Cem. Concr. Res.* **2006**, *36*, 1263–1267. [[CrossRef](#)]
37. Ma, Y.; Qiu, J.; Wang, P.; Yang, Q.B.; Sun, Z.P.; Jiang, Z.W. Effect of polypropylene fiber on the plastic shrinkage stress and plastic shrinkage ratio of mortar. *J. Build. Mater.* **2005**, *8*, 499–507.
38. Zeiml, M.; Leithner, D.; Lackner, R.; Mang, H.A. How do polypropylene fibers improve the spalling behavior of in-situ concrete. *Cem. Concr. Res.* **2006**, *36*, 929–942. [[CrossRef](#)]
39. Zhang, P.; Li, Q.; Zhang, H. Combined effect of polypropylene fiber and silica fume on mechanical properties of concrete composite containing fly ash. *J. Reinf. Plast. Compos.* **2011**, *30*, 1349–1358. [[CrossRef](#)]
40. Benzaazoua, M.; Fall, M.; Belem, T. A contribution to understanding the hardening process of cemented pastefill. *Miner. Eng.* **2004**, *17*, 141–152. [[CrossRef](#)]
41. Alexander, M.G. Effects of aging on mechanical properties of the interfacial zone between cement paste and rock. *Cem. Concr. Res.* **1994**, *24*, 1277–1285. [[CrossRef](#)]
42. Yi, X.W.; Ma, G.W.; Fourie, A. Compressive behaviour of fibre-reinforced cemented paste backfill. *Geotext. Geomembr.* **2015**, *43*, 207–215. [[CrossRef](#)]
43. Consoli, N.C.; Zorzea, F.; Souza, M.D.; Festugato, L. Studies on the dosage of fiber-reinforced cemented soils. *J. Mater. Civ. Eng.* **2011**, *23*, 1624–1632. [[CrossRef](#)]
44. Zaimoglu, A.S.; Yetimoglu, T. Strength behavior of fine grained soil reinforced with randomly distributed polypropylene fibers. *Geotech. Geol. Eng.* **2012**, *30*, 197–203. [[CrossRef](#)]
45. Miller, G.A.; Hamid, T.B. Interface direct shear testing of unsaturated soil. *Geotech. Test. J.* **2006**, *30*, 182–191.
46. Fall, M.; Pokharel, M. Coupled effects of sulphate and temperature on the strength development of cemented tailings backfills: Portland cement-paste backfill. *Cem. Concr. Compos.* **2010**, *32*, 819–828. [[CrossRef](#)]

47. Tzouvalas, G.; Dermatas, N.; Tsimas, S. Alternative calcium sulfate-bearing materials as cement retarders: Part I. Anhydrite. *Cem. Concr. Res.* **2004**, *34*, 2113–2118. [[CrossRef](#)]
48. Orejarena, L.; Fall, M. Artificial neural network based modeling of the coupled effect of sulphate and temperature on the strength of cemented paste backfill. *Rev. Can. Génie Civ.* **2011**, *38*, 100–109. [[CrossRef](#)]
49. Gani, M.S.J. *Cement and Concrete*; Chapman and Hall: London, UK, 1997.
50. Kyungsu, H.; Habeun, C.; Moochul, S.; Park, K. On the size effect of interfacial fracture between concrete and fiber reinforced polymer. *Cem. Concr. Compos.* **2018**, *93*, 99–106.
51. Karthik, M.P.; Maruthachalam, D. Experimental study on shear behaviour of hybrid Fibre Reinforced Concrete beams. *KSCE J. Civ. Eng.* **2015**, *19*, 259–264. [[CrossRef](#)]
52. Correia, A.A.S.; Venda Oliveira, P.J.; Custodio, D.G. Effect of polypropylene fibres on the compressive and tensile strength of a soft soil, artificially stabilised with binders. *Geotext. Geomembr.* **2015**, *43*, 97–106. [[CrossRef](#)]
53. Li, W.; Fall, M. Sulphate effect on the early age strength and self-desiccation of cemented paste backfill. *Constr. Build. Mater.* **2016**, *106*, 296–604. [[CrossRef](#)]
54. Chen, X.; Shi, X.; Zhou, J.; Yu, Z. Influence of polypropylene fiber reinforcement on tensile behavior and failure mode of tailings cemented paste backfill. *IEEE Access* **2019**, *7*, 69015–69026. [[CrossRef](#)]
55. Tang, C.; Shi, B.; Gao, W.; Chen, F.; Cai, Y. Strength and mechanical behavior of short polypropylene fiber reinforced and cement stabilized clayey soil. *Geotext. Geomembr.* **2007**, *25*, 194–202. [[CrossRef](#)]
56. Xu, X.; Fall, M.; Alainachi, I.; Fang, K. Characterization of fiber-reinforced backfill/rock interface through direct shear Tests. *Geotech. Res.* **2020**, *7*, 11–25. [[CrossRef](#)]
57. Ercikdi, B.; Kesimal, A.; Cihangir, F.; Deveci, H.; Alp, İ. Cemented paste backfill of sulphide-rich tailings: Importance of binder type and dosage. *Cem. Concr. Compos.* **2009**, *31*, 268–274. [[CrossRef](#)]
58. Saiang, D.; Malmgren, L.; Nordlund, E. Laboratory tests on shotcrete-rock joints in direct shear, tension and compression. *Rock Mech. Rock Eng.* **2005**, *38*, 275–297. [[CrossRef](#)]
59. Tian, H.; Chen, W.; Yang, D.; Yang, J.P. Experimental and numerical analysis of the shear behaviour of cemented concrete–rock joints. *Rock Mech. Rock Eng.* **2015**, *48*, 213–222. [[CrossRef](#)]
60. Pane, I.; Hansen, W. Investigation of blended cement hydration by isothermal calorimetry and thermal analysis. *Cem. Concr. Res.* **2005**, *35*, 1155–1164. [[CrossRef](#)]
61. Fall, M.; Benzaazoua, M.; Ouellet, S. Experimental characterization of the influence of tailings fineness and density on the quality of cemented paste backfill. *Miner. Eng.* **2005**, *18*, 41–44. [[CrossRef](#)]
62. Fall, M.; Pokharel, M. Strength development and sorptivity of tailings shotcrete under various thermal and chemical loads. *Can. J. Civ. Eng.* **2011**, *38*, 772–784.
63. Mota, B.; Matschei, T.; Scrivener, K. The influence of sodium salts and gypsum on alite hydration. *Cem. Concr. Res.* **2015**, *75*, 53–65. [[CrossRef](#)]
64. Bentur, A. Effect of gypsum on the hydration and strength of C₃S Pastes. *Cheminform* **1976**, *59*, 210–214. [[CrossRef](#)]
65. Pelisser, F.; Gleize, P.J.P.; Mikowski, A. Effect of the Ca/Si molar ratio on the micro/nanomechanical properties of synthetic C-S-H measured by nanoindentation. *J. Phys. Chem. C* **2012**, *116*, 17219–17227. [[CrossRef](#)]
66. Xu, W.; Cao, P.; Tian, M. Strength Development and Microstructure Evolution of Cemented Tailings Backfill Containing Different Binder Types and Contents. *Minerals* **2018**, *8*, 167. [[CrossRef](#)]
67. Hou, D.; Zhang, J.; Li, Z.; Zhu, Y. Uniaxial tension study of calcium silicate hydrate (C–S–H): Structure, dynamics and mechanical properties. *Mater. Struct.* **2015**, *48*, 3811–3824. [[CrossRef](#)]
68. Kantro, D.L.; Brunauer, S.; Weise, C.H. Development of surface in the hydration of calcium silicate in solid surfaces and the gas-solid interface. *Adv. Chem.* **1961**, *33*, 199–219.
69. Li, W.; Fall, M. Strength and self-desiccation of slag-cemented paste backfill at early ages: Link to initial sulphate concentration. *Cem. Concr. Compos.* **2018**, *89*, 160–168. [[CrossRef](#)]
70. Prabakar, J.; Sridhar, R.S. Effect of random inclusion of sisal fibre on strength behaviour of soil. *Constr. Build. Mater.* **2002**, *16*, 123–131. [[CrossRef](#)]
71. Consoli, N.C.; Bassani, M.A.A.; Festugato, L. Effect of fiber reinforcement on the strength of cemented soils. *Geotext. Geomembr.* **2010**, *28*, 344–351. [[CrossRef](#)]
72. Xu, W.; Li, Q.; Zhang, Y. Influence of temperature on compressive strength, microstructure properties and failure pattern of fiber-reinforced cemented tailings backfill. *Constr. Build. Mater.* **2019**, *222*, 776–785. [[CrossRef](#)]

73. Cao, S.; Zheng, D.; Yilmaz, E.; Yin, Z.; Xue, G.; Yang, F. Strength development and microstructure characteristics of artificial concrete pillar considering fiber type and content effects. *Constr. Build. Mater.* **2020**, *256*, 119408. [[CrossRef](#)]
74. Starcher, R.D.; Liu, C. Mechanical behavior of cement- and cement-fiber-improved soft soils. In *Geo-Congress 2013: Stability and Performance of Slopes and Embankments III*; Meehan, C., Pradel, D., Pando, M.A., Labuz, J.F., Eds.; American Society of Civil Engineers: Reston, VA, USA, 2013; pp. 2048–2057.

Publisher’s Note: MDPI stays neutral with regard to jurisdictional claims in published maps and institutional affiliations.



© 2020 by the authors. Licensee MDPI, Basel, Switzerland. This article is an open access article distributed under the terms and conditions of the Creative Commons Attribution (CC BY) license (<http://creativecommons.org/licenses/by/4.0/>).